

Supporting information for Time-varying drainage basin development and erosion on volcanic edifices

Daniel O'Hara¹, Liran Goren², Roos M.J. van Wees¹, Benjamin Campforts³, Pablo Grosse^{4,5}, Pierre Lahitte⁶, Gabor Kereszturi⁷, Matthieu Kervyn¹

¹Department of Geography, Vrije Universiteit Brussel, Pleinlaan 2, 1050 Elsene.

² Ben Gurion University of the Negev, Department of Earth and Environmental Sciences, Beer-Sheva, Israel

³ Institute of Arctic and Alpine Research, University of Colorado Boulder, Boulder, CO, USA

⁴ Consejo Nacional de Investigaciones Científicas y Técnicas (CONICET), Argentina

⁵ Fundación Miguel Lillo, Miguel Lillo 251, (4000) Tucumán, Argentina

⁶ Université Paris-Saclay, CNRS, Laboratoire GEOPS, Rue du Belvédère, 91405 Orsay, France

⁷ Volcanic Risk Solutions, School of Agriculture and Environment, Massey University, 4474, New Zealand

1.0 Introduction

In the main text, we describe our analyses of drainage development on volcanic edifices, propose a new conceptual model for edifice degradation, and discuss the complexity of drainage competition on radial landforms. Below, we provide supplemental information related to the main text, including sensitivity analysis for the drainage density and Hack's Law relationships described in the main text, metric regression values for linear-mean edifice ages, temporal relationships of non-normalized summit basin numbers, and a summary of edifice age and morphology data.

2.0 Hack's Law derivation

In the main text, we derive basin lengths for Hack's power-law relationship using mid-point basin lengths, as opposed to the flow path length that is typically used. Although this choice is made to remove the effects of channel sinuosity, Fig. S1 demonstrates that it creates only slightly different exponent values. The exponential regression between the Hack's Law exponent and time have nearly equal values, and correlation R^2 values are approximately the same.

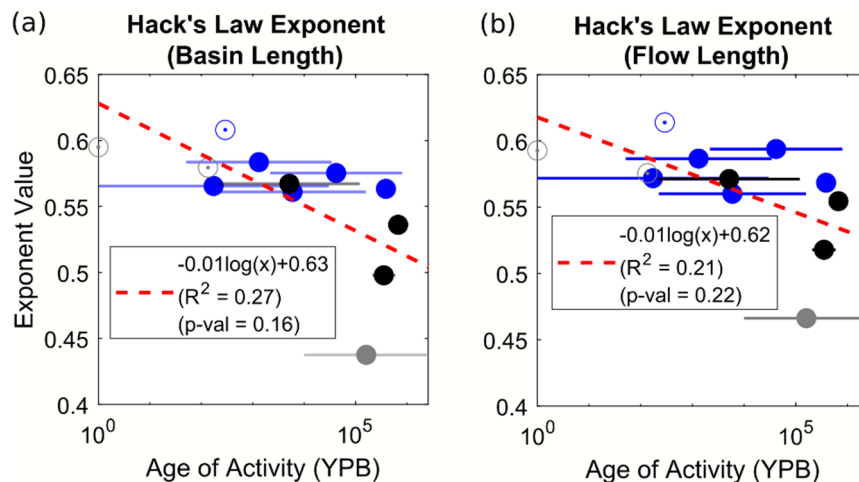


Figure S1 – Temporal relationships of Hack's Law exponent derived using (a) mid-point basin lengths and (b) flow path lengths. Symbols and colors described in Figs. 3 and 4. Red-dashed lines are logarithmic regressions (equations described in legends); open circles are excluded in the regression due to age limitations.

3.0 Drainage area thresholds for channelization, and drainage density and Hack's Law sensitivity tests

To calculate Hack's Law and drainage density, we first need to make an assumption on basin sizes that allow fluvial networks to form. We use a common method to determine fluvial basins by assuming basins with an upstream drainage area greater than some threshold support channelization (Montgomery and Dietrich, 1989). For consistency across all edifices, we use the same drainage area threshold. To determine the best threshold drainage area, we conduct an automated slope-area analysis of summit basin longest flow paths. Drainage channels are defined by a distinct power-law between upstream drainage area and slope that 1) is negatively-correlated, as opposed to positively-correlated relationships related to hillslopes, and 2) have more negative exponent values (i.e., steeper slope in log-log) than valley heads and colluvial channels (Montgomery, 2001).

Our automated algorithm determines the best-fit drainage area threshold for channelization through a series of regression analyses. Using 20-pixel steps (0.018 km² area for a 30-m grid resolution), the algorithm first performs a power-law regression of the slope-area data from the divide to each step. From this, the algorithm determines the extent of the hillslope based on where the power-law exponent changes from positive to negative values. Afterwards, the algorithm performs a coupled regression analysis. Moving from the hillslope extent in 20-pixel steps, the algorithm conducts a power-law regression on the slope-area data between the pixel step and hillslope extent, as well as a power-law regression on the data between the pixel step and the highest drainage area. The goal of this is to both maximize the fit of individual regressions, while also minimizing the difference between them. The algorithm thus determines the best drainage area threshold by finding the largest r' value, defined as

$$r' = \frac{\min(r_1, r_2)}{\max(r_1, r_2)} * \frac{r_1 + r_2}{2}, \quad (\text{E1})$$

where r_1 and r_2 are the R^2 values of both regressions. Equation E1 thus produces a maximum value for r' of 1.

We find automated drainage area thresholds ranging 0.32 – 1.42 km², with a mean value of 0.78 km² (Table T1). Considering specific examples (Fig. S2a-b), the automated algorithm is able to recognize the break in slope-area trends between fluvial and colluvial regimes; however, the algorithm often overestimates the location where this break occurs (e.g., Sumbing; Fig. S2b). Furthermore, as shown at Kaitake (Fig. S2c), the assumption that fluvial and colluvial regimes have recognizable differences in slope-area is not always true, and the algorithm struggles to find an appropriate threshold.

Table T1 – Best-fit drainage area thresholds for edifices in this study, based on automated slope-area regression. r_1 and r_2 are R^2 regression values of determined colluvial and fluvial regimes. r' is calculated by eq. E1.

Volcano	Best-Fit Area Threshold (km ²)	r_1	r_2	r'
Bamus	0.68	0.21	0.21	0.21
Kaitake	N/A	N/A	N/A	N/A
Likuruanga	0.35	0.23	0.23	0.23
Merapi	0.68	0.2	0.2	0.20
Merbabu	1.24	0.18	0.18	0.18
Muria	0.46	0.24	0.24	0.24
Pouakai	0.59	0.2	0.2	0.19
Sumbing	1.42	0.23	0.24	0.23
Sundoro	1.05	0.24	0.24	0.24
Taranaki	0.72	0.24	0.24	0.24
Ulawun	0.32	0.3	0.31	0.30
Ungaran	1.06	0.14	0.14	0.14
Mean:	0.78			

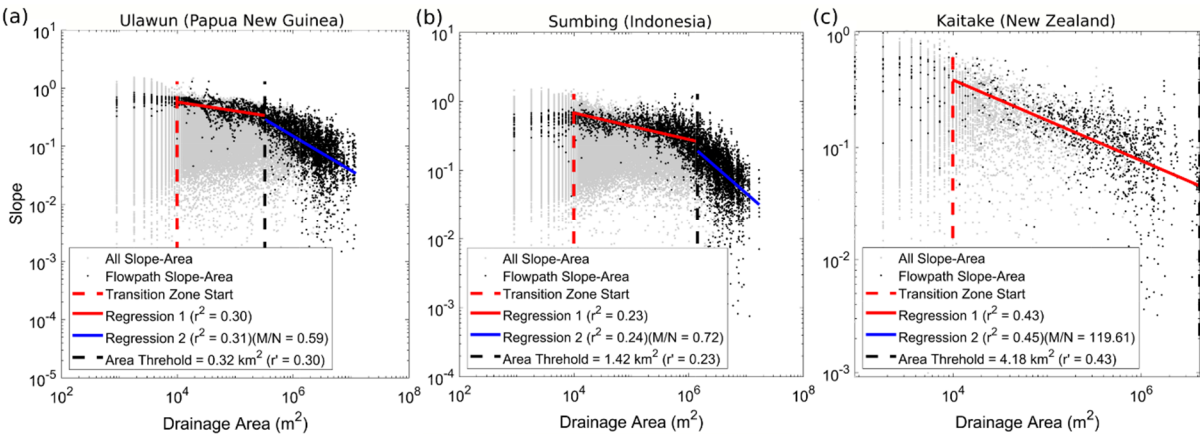


Figure S2 – Slope-area regression results for (a) Ulawun, (b) Sumbing, and (c) Kaitake edifice summit basins. Gray dots are all summit basin slope-area values; black lines are slope-area values of only the longest basin flow paths. Red and blue lines distinguish determined colluvial and fluvial regimes, respectively. Red-dashed line is transition zone between hillslopes and colluvial regime, black-dashed line is determined threshold for channelization.

Our automated algorithm suggests the mean drainage area threshold for channelization across all edifices is 0.78 km²; however, to account for the overestimation in drainage area threshold that our algorithm can produce, and to ensure that the channel network of the smallest edifices can be properly accounted for, we round this threshold down to 0.5 km². Thus, basins that are used for the Hack's Law analysis and flowpaths that are used for the drainage density analysis are only those that have an upstream drainage area greater than 0.5 km². We test the impact of this threshold on our results through a sensitivity test. To do this, DrainageVolc is ran for all edifice sets from Indonesia, New Guinea, and New Zealand (Fig. 1) with different drainage area thresholds of 0.1 km², 0.5 km², and 1.0 km², as

well as the best-fit channelization threshold for each edifice. We then fit logarithmic regressions to the relationships between Hack's Law exponent, drainage density, and log-mean edifice age.

Fig. S3 shows the results of this analysis. Regardless of channelization threshold, drainage density always experiences a temporally-decreasing trend. Furthermore, considering the constant drainage area threshold analysis (Fig. S3a-c), drainage density consistently decreases with increasing thresholds. This is not surprising, as increasing drainage area threshold removes basin interfluvies from the analysis, thus generating lower cumulative channel lengths. R^2 values remain above 0.4 for all thresholds; however, these values also decrease with increasing drainage area thresholds, suggesting the relationship described in the main text becomes weaker when considering the main channels of the edifice drainage network. In the case of variable drainage area threshold (Fig. S3d), both drainage density and regression values are similar to using a constant 1.0 km² area threshold; however, R^2 values are lower (0.2), suggesting this relationship becomes weaker.

Temporal trends with the Hack's Law exponent are much more sensitive to the channelization threshold (Fig. S3e-h). Using only basins defined by an upstream drainage area of 0.1 km², or letting the automatized algorithm choose the best-fitting channelization threshold for each edifice, produces no correlation with edifice age; whereas upstream drainage area thresholds of 1.0 km² produces the strongest relationship. These differences between drainage area threshold and temporal correlation are indicative of smaller drainage area thresholds incorporating more non-fluvial basin within the analysis that can significantly alter the Hack's Law regression (e.g., Figs. 2b, 9a, c).

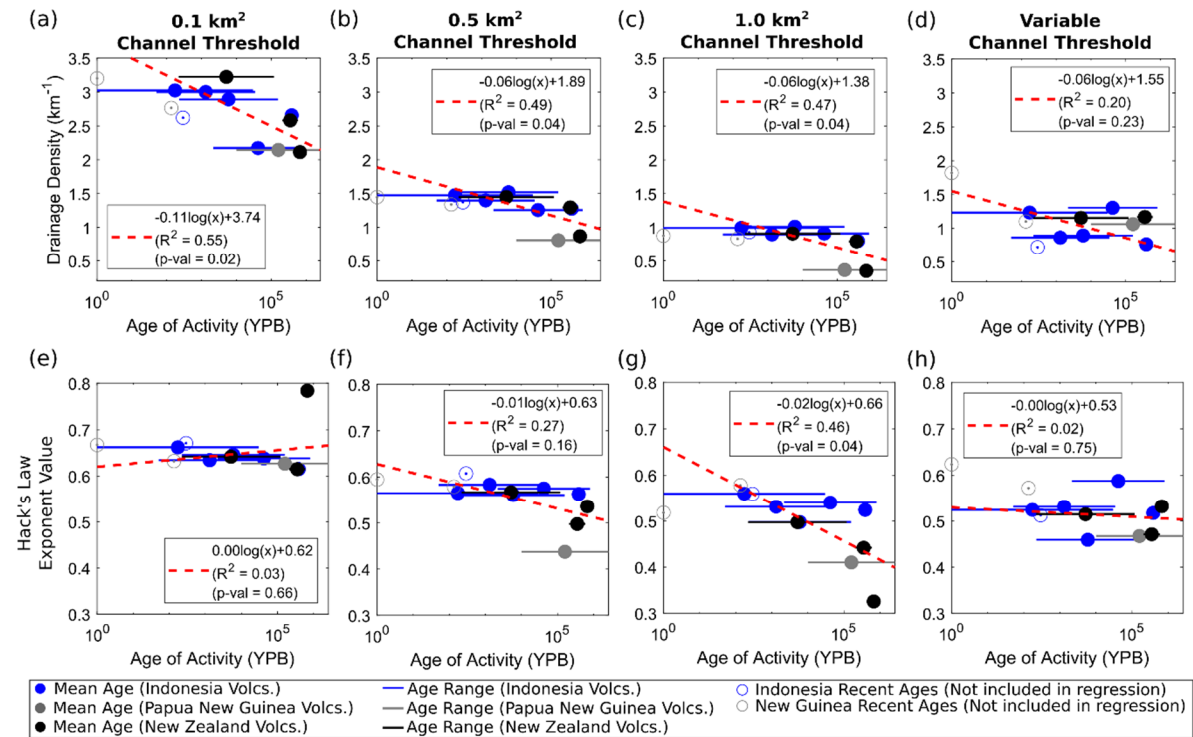


Figure S3 – (a-d) Drainage density and (e-h) Hack's Law relationships with log-mean edifice age for different values of the upstream drainage area threshold for channelization. Symbols and colors described in bottom legend. Red-dashed lines are logarithmic regressions (equations described in legends); open circles are excluded in the regression due to age limitations.

4.0 Characteristic basins defined by radial distance

Our analysis of basin geometries through time assumes that the larger basins that exist on an edifice are most characteristic of overall basin morphology and evolution. In the main text, we define these characteristic basins as those that reach the upper 30% of the edifice's height. However, characteristic basins may also be defined as those that are within some distance from the edifice's peak. We test the impact of our elevation-based definition of characteristic basins to a distance-based definition by conducting a regression analysis similar to that in the main text. For this, we transform the Cartesian DEM grid into radial coordinates relative to the edifice's highest topography, and normalize these values by the maximum radial distance to the boundary. Following the process described in Section 3.2 of the main text, we then isolate basins that extend to within 30% normalized distance of the edifice's peak and analyze their geometries. Fig. S4 shows the temporal regression results of these characteristic basin morphologies.

Normalized basin lengths and the number of radial basins normalized by the radial distance contour show no correlation with edifice age. This lack of correlation is expected as the definition for choosing these basins already incorporates a distance normalization, and thus these metrics become irrelevant. The temporal correlation with mean basin relief becomes weaker ($R^2 = 0.26$) for radial distance-based characteristic basins compared to elevation-based (Fig. 3); whereas the mean basin slope becomes stronger (though still an overall weak correlation; $R^2 = 0.37$). However, mean basin hypsometry integral and normalized basin widths still experience strong correlations with time ($R^2 = 0.62$ for both), suggesting that these metrics are moderately insensitive to characteristic basin definition, further demonstrating that these geometries are strong indicators for the edifice's erosional maturity.

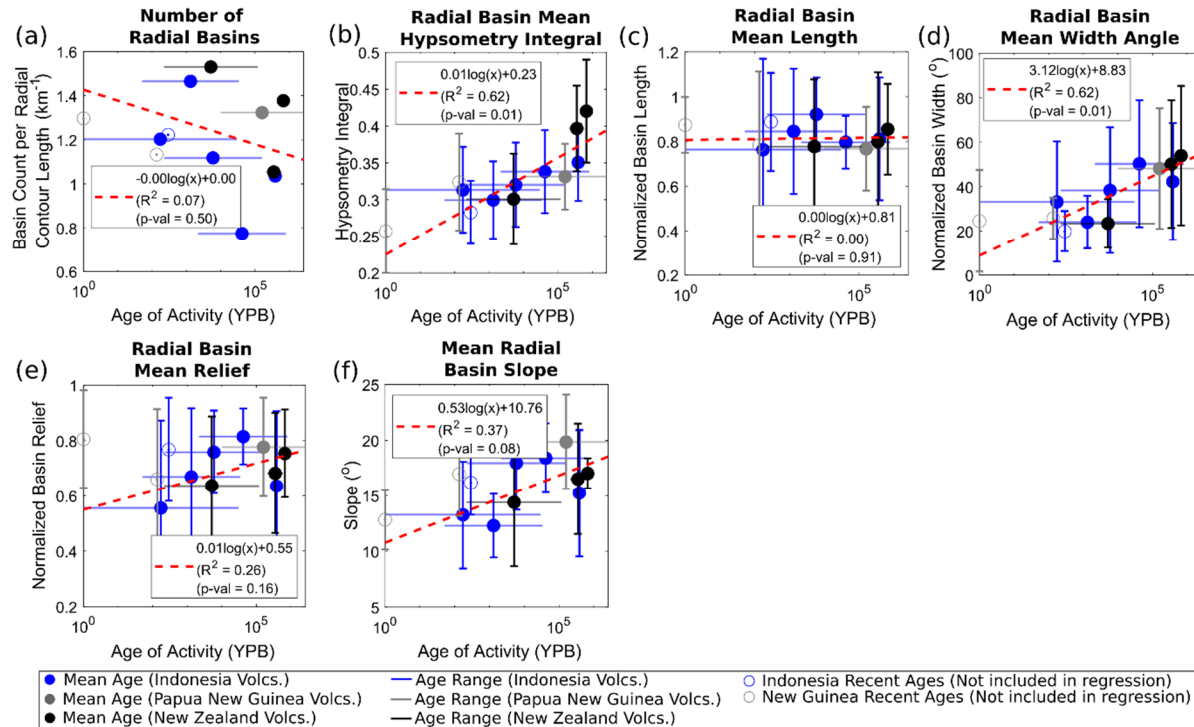


Figure S4 - Temporal relationships of basin morphology metrics using a radial distance-based definition for characteristic basins. Symbols and colors described in legend. Vertical lines represent standard deviations of values (where appropriate). Red-dashed lines are logarithmic regressions (equations described in legends); open circles are excluded in the regression due to age limitations.

5.0 Edifice Age

Within the main text, we analyzed the temporal relationships of edifice basin geometries. In order to account for the large temporal span of events that can alter edifice morphology (short-term volcanic episodes and long-term degradation processes) within a single value, we quantified the edifice's age as the log-mean value between its known most recent eruption and age of initiation. To verify that this selection does not impact our results, we also present the logarithmic regressions of the basin metrics using the linear mean age of the edifice.

Fig. S5 shows that the linear mean ages create overall similar regression values as the log-mean ages. Drainage density, normalized number of summit basins, normalized mean summit basin length, normalized mean summit basin width, mean summit basin slope, edifice relief, relief-width ratio, mean irregularity index, and eroded volume percentages all have better regression fits when using linear mean ages; while Hack's Law exponent, mean summit basin hypsometry integral, mean normalized summit basin relief, edifice effective radius, main flank mean slope, mean ellipticity index, and slope variance have better regression fits for the log-mean ages.

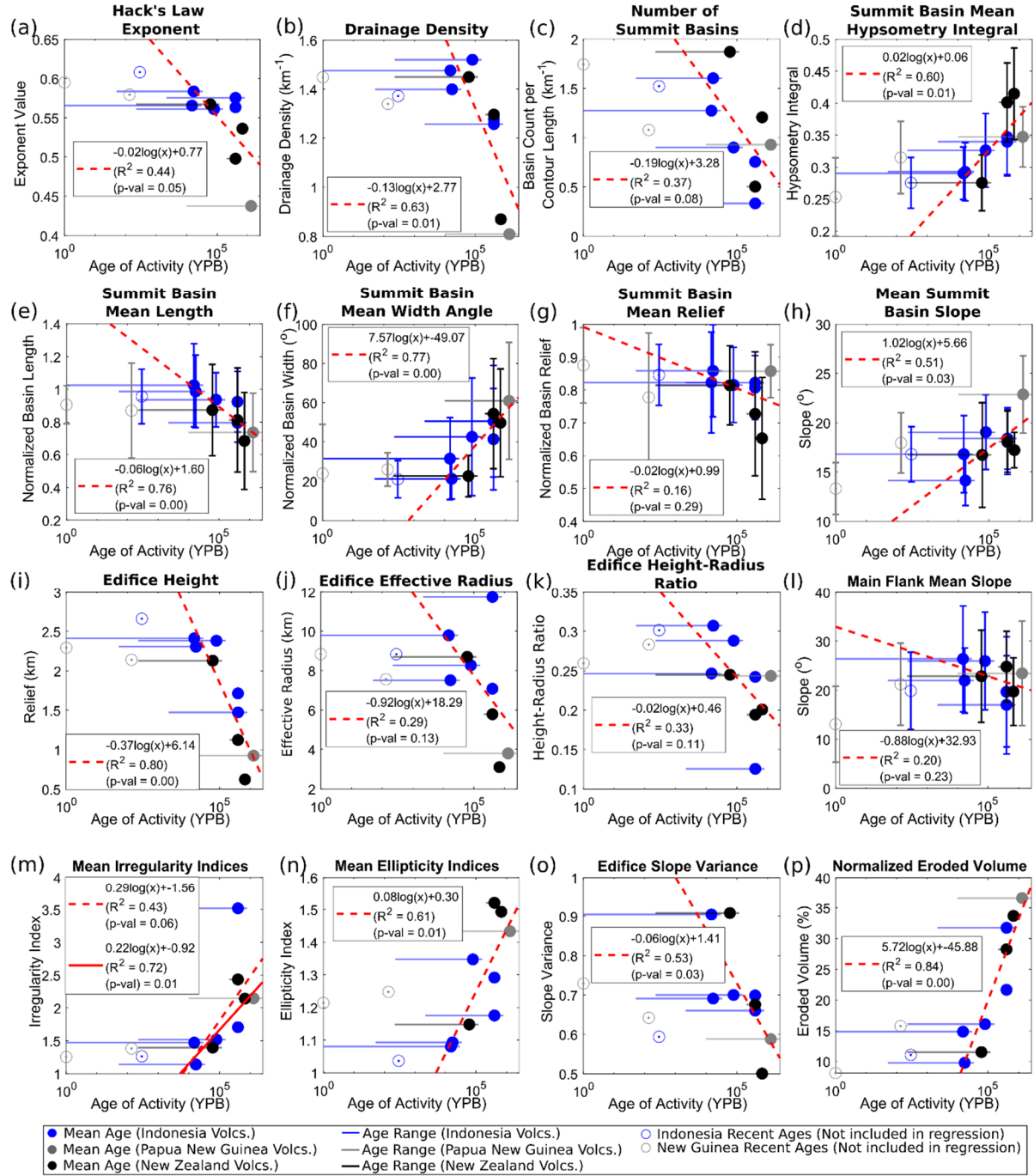


Figure S5 – Temporal relationships of morphology metrics using linear mean edifice ages. Symbols and colors described in legend. Vertical lines represent standard deviations of values (where appropriate). Red-dashed lines are logarithmic regressions (equations described in legends); open circles are excluded in the regression due to age limitations.

6.0 Summit and Radial-Distance Basin Numbers

Fig. S6 shows the non-normalized number of summit basins for different summit designations (upper 20%, 10%, and 5% of relief) discussed in the main text. Weak or no correlations exist between number of summit basins and time when considering basins that exist in the upper 30% - 10% of the edifice's height (Figs. 7b, S5a-b); however, a

higher correlation ($R^2 = 0.42$) does exist when considering the strictest summit designation (upper 5% of edifice height).

In comparison, the number of basins at normalized radial distances from the edifice's peak (Fig. S7) shows strong correlations with time for all considered distances (20%, 50%, and 70%), with higher basin counts occurring at larger distances.

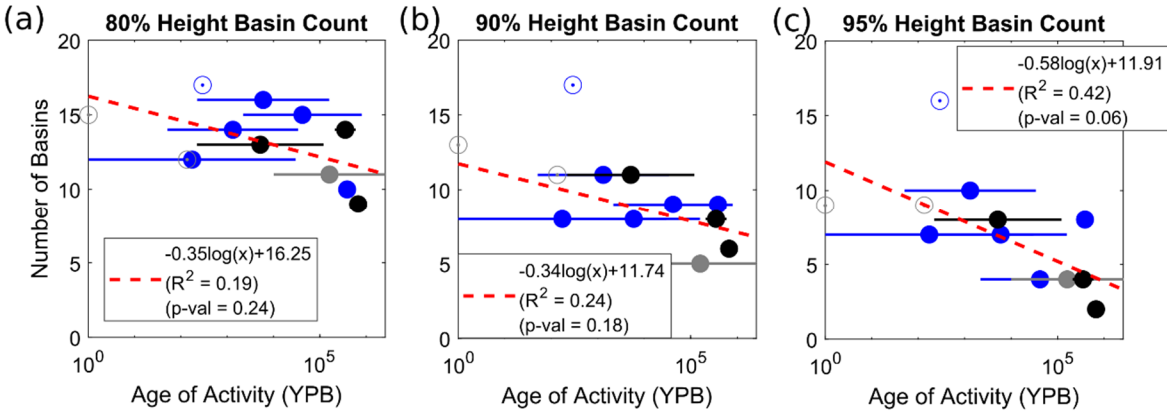


Figure S6 – Temporal relationships of the raw number of summit basins for upper (a) 20%, (b) 10%, and (c) 5% of edifice relief. Symbols and colors described in legend of Fig. 3. Red-dashed lines are logarithmic regressions (equations described in legends); open circles are excluded in the regression due to age limitations.

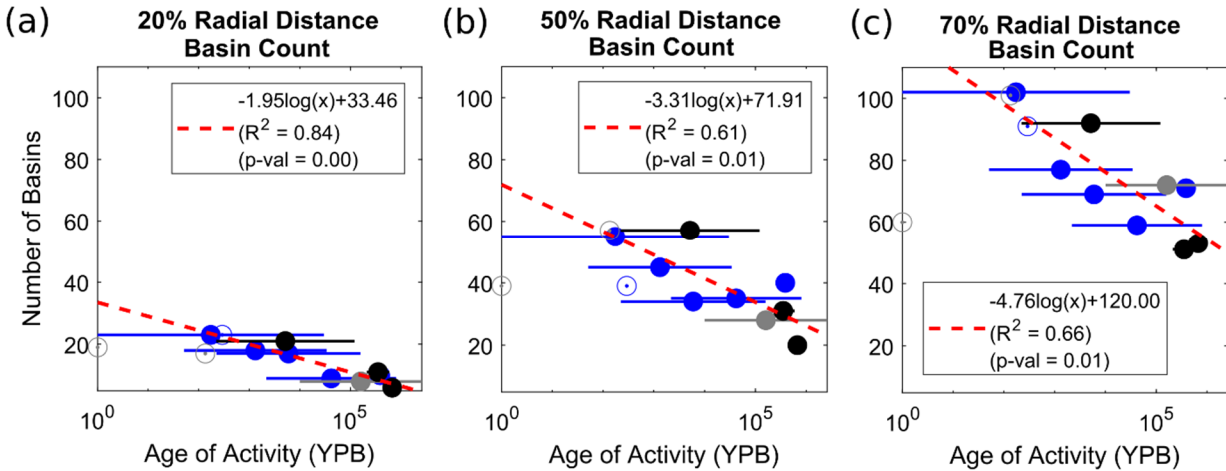


Figure S7 – Temporal relationships of the raw number of basins for (a) 20%, (b) 50%, and (c) 70% of normalized distance from edifice peak. Symbols and colors described in legend of Fig. 3. Red-dashed lines are logarithmic regressions (equations described in legends); open circles are excluded in the regression due to age limitations.

7.0 Edifice Age Data

Supplementary Table T3 gives a compilation of known minimum and maximum ages of volcanic activity for the analyzed volcanoes, their associated references, and a summary of morphologic data from DrainageVolc and MorVolc presented here. The supplementary shapefile provides the same information, as well as the XY data of edifice boundaries. Table T2 below is a shortened version of Table T3 providing edifice ages and their sources.

Table T2 – Age data and references for the edifices analyzed in the main text.

<u>Region</u>	<u>Volcano</u>	<u>Minimum Known Age of Activity (YBP)</u>	<u>Maximum Known Age of Activity (YBP)</u>	<u>Log-Mean Activity Age (YBP)</u>	<u>Reference</u>
Indonesia	Merapi	1	30,000	173	(Gertisser et al., 2012; Global Volcanism Program, 2013)
Indonesia	Merbabu	224	158,000	5,949	(Gomez et al., 2010; Global Volcanism Program, 2013)
Indonesia	Ungaran	300,000	500,000	387,298	(Kohn, 2006)
Indonesia	Muria	2,181	800,000	41,771	(McBirney et al., 2003; Global Volcanism Program, 2013)
Indonesia	Sumbing	292	N/A	N/A	(Global Volcanism Program, 2013)
Indonesia	Sundoro	51	34,000	1,317	(Prambada et al., 2016; Global Volcanism Program, 2013)
New Guinea	Bamus	135	N/A	N/A	(Global Volcanism Program, 2013)
New Guinea	Ulawun	1	N/A	N/A	(Global Volcanism Program, 2013)
New Guinea	Likuruanga*	10,000 (Pleistocene)	2,580,000 (Pleistocene)	160,623	(Global Volcanism Program, 2013)
New Zealand	Taranaki	221	120,000	5,150	(Neall, 1979; Locke et al., 1993)
New Zealand	Pouakai	210,000	590,000	351,994	(Neall, 1979; Gaylord and Neall, 2012)
New Zealand	Kaitake	590,000	760,000	669,627	(Neall, 1979; Gaylord and Neall, 2012)

* Relative age (non-radiometric). For consistency, log-mean Pleistocene age is used for regression in main text (Figs. 3-8).

8.0 References

- Gaylord, D. R. and Neall, V. E.: Subedifice collapse of an andesitic stratovolcano: The maitahi formation, Taranaki Peninsula, New Zealand, *Bull. Geol. Soc. Am.*, 124, 181–199, <https://doi.org/10.1130/B30141.1>, 2012.
- Gertisser, R., Charbonnier, S. J., Keller, J., and Quidelleur, X.: The geological evolution of Merapi volcano, Central Java, Indonesia, *Bull. Volcanol.*, 74, 1213–1233, <https://doi.org/10.1007/s00445-012-0591-3>, 2012.
- Global Volcanism Program: Volcanoes of the World, v. 4.10.5 (27 Jan 2022), *Smithson. Inst.*, 2013.
- Gomez, C., Janin, M., Lavigne, F., Gertisser, R., Charbonnier, S., Lahitte, P., Hadmoko, S. R., Fort, M., Wassmer, P., Degroot, V., and Murwanto, H.: Borobudur, a basin under volcanic influence: 361,000 years BP to present, *J. Volcanol. Geotherm. Res.*, 196, 245–264, <https://doi.org/10.1016/j.jvolgeores.2010.08.001>, 2010.
- Kohno, Y.: Geological and geochemical study on the Ungaran geothermal field, Central Java, Indonesia: an implication in genesis and nature of geothermal water and heat source, in: *Proceedings of 4th International Workshop on Earth Science and Technology*, 367–374, 2006.
- Locke, C. A., Cassidy, J., and MacDonald, A.: Three-dimensional structure of relict stratovolcanoes in Taranaki, New Zealand: evidence from gravity data, *J. Volcanol. Geotherm. Res.*, 59, 121–130, [https://doi.org/10.1016/0377-0273\(93\)90081-2](https://doi.org/10.1016/0377-0273(93)90081-2), 1993.
- McBirney, A. R., Serva, L., Guerra, M., and Connor, C. B.: Volcanic and seismic hazards at a proposed nuclear power site in central Java, *J. Volcanol. Geotherm. Res.*, 126, 11–30, [https://doi.org/10.1016/S0377-0273\(03\)00114-8](https://doi.org/10.1016/S0377-0273(03)00114-8), 2003.
- Montgomery, D. R.: Slope distributions, threshold hillslopes, and steady-state topography, *Am. J. Sci.*, 301, 432–454, <https://doi.org/10.2475/ajs.301.4-5.432>, 2001.
- Montgomery, D. R. and Dietrich, W. E.: Source Areas, Drainage Density, and Channel Initiation, *Water Resour. Res.*, 25, 1907–1918, 1989.
- Neall, V. E.: Sheets P19, P20, ad P21 New Plymouth, Egmont and Manaia: Geological Map of New Zealand: Wellington, 36 pp., 1979.
- Prambada, O., Arakawa, Y., Ikehata, K., Furukawa, R., Takada, A., Wibowo, H. E., Nakagawa, M., and Kartadinata, M. N.: Eruptive history of Sundoro volcano, Central Java, Indonesia since 34 ka, *Bull. Volcanol.*, 78, <https://doi.org/10.1007/s00445-016-1079-3>, 2016.